ISSN 0208-7774 TRIBOLOGIA 1/2024 p. 147–158
DOI: 10.5604/01.3001.0054.4668

Małgorzata WITKOWSKA[*], Joanna KOWALSKA[**], Kinga CHRONOWSKA-PRZYWARA[***]

ANALYSIS OF THE MICROSTRUCTURE AND MECHANICAL PROPERTIES OF DUPLEX STEEL JOINTS

ANALIZA MIKROSTRUKTURY I WŁASNOŚCI MECHANICZNYCH ZŁĄCZY STALI DUPLEX

Key words: duplex steel, microhardness, microstructure, wear resistance, coefficient of friction.

Summary: The article presents a study, the aim of which was to analyze the microstructure and mechanical properties of welded joints of austenitic-ferritic duplex steel X2CrMnNiN21-5-1. This steel is characterized by good resistance to various types of corrosion, good strength properties and good weldability. Due to all these advantages, it is used in many industry sectors, and the main joining techniques are welding technologies. In this study, two joining techniques were used, SMAW (Shielded Metal Arc Welding) and GTA (Gas Tungsten Arc). The obtained welded joints were subjected to: macroscopic and microscopic metallographic tests, mechanical tests (static bending test and microhardness measurements), diffraction tests, and wear resistance tests. The results showed that the microhardness of the welds is similar and does not depend on the welding method used. In the microstructure of the analyzed joints there are two phases: austenite (γ) and ferrite (δ), with different morphologies depending on the welding conditions, which affect the phase transformations. Material wear within the weld is greater than in the base material.

Słowa kluczowe: stal typu duplex, mikrotwardość, mikrostruktura, odporność na zużycie, współczynnik tarcia.

Streszczenie: Celem badań była analiza mikrostruktury i własności mechanicznych złączy spawanych stali austenityczno-ferrytycznej typu duplex X2CrMnNiN21-5-1. Stal ta charakteryzuje się dobrą odpornością na różnego rodzaju korozje, dobrymi własnościami wytrzymałościowymi i dobrą spawalnością. Dzięki tym wszystkim zaletom znajduje zastosowanie w wielu gałęziach przemysłu, a głównymi technikami jej łączenia są technologie spawalnicze. W pracy zastosowano dwie techniki łączenia metodą SMAW (Shielded Metal Arc Welding) i GTA (Gas Tungsten Arc). Uzyskane złącza spawane poddano: badaniom metalograficznym makro- i mikroskopowym, badaniom mechanicznym (statyczna próba zginania i pomiary mikrotwardości), badaniom dyfrakcyjnym oraz badaniom odporności na zużycie. Wyniki badań pokazały, że mikrotwardości spoin są zbliżone i nie zależą od zastosowanej metody spawania. W mikrostrukturze analizowanych złącz występują dwie fazy austenit (γ) i ferryt (δ) o zróżnicowanej morfologii zależnej od warunków spawania, które wpływają na przemiany fazowe. Zużycie materiału w obrębie spoiny jest większe aniżeli w materiale rodzimym.

INTRODUCTION

Trends in the development of alloy steels with special properties are aimed at obtaining iron alloys that combine the advantages of austenitic and ferritic steels. These are highly corrosion-resistant alloyed steels that, due to appropriate chemical composition and heat treatment austenite, have a structure composed of two phases of ferrite and austenite. Most designed alloys contain approximately equal amounts of both phases after annealing, hence the name duplex stainless steels. In practice, the properties of duplex steels depend on the two-phase microstructure, which is affected

[*] ORCID: 0000-0002-3157-6462. AGH University of Krakow, Faculty of Metals Engineering and Industrial Computer Science, Mickiewicza 30 Ave., 30-059 Krakow, Poland.
[**] ORCID: 0000-0003-1008-2794. AGH University of Krakow, Faculty of Metals Engineering and Industrial Computer Science, Mickiewicza 30, Ave., 30-059 Krakow, Poland.
[***] ORCID: 0000-0003-3510-4443. AGH University of Krakow, Faculty of Mechanical Engineering and Robotics, Mickiewicza 30, Ave., 30-059 Krakow, Poland.

by the chemical composition and the applied heat treatment **[L. 1–3]**. In the 1970s, research began on improving the properties of corrosion-resistant steels. Progress was mainly achieved by suitably modifying the chemical composition in order to reduce the price and obtain even better strength and weldability properties. This research resulted in the development of Lean, Super duplex and Hyper duplex steels **[L. 4, 5]**. Currently produced duplex steels contain 20–28% Cr, 3–8% Ni, up to 4.5% Mo, 0.08–0.35% N, up to 0.03%C and W and Cu additives. It is important to keep the carbon and nitrogen content at an appropriate level. The carbon content should not exceed 0.03% due to the steel's tendency to form carbides and the danger of intergranular corrosion. Nitrogen, on the other hand, has a very beneficial effect on the properties of duplex steels: it improves strength, corrosion resistance and weldability, and contributes to phase stability. Duplex steels are characterized by high mechanical properties: yield strength, tensile strength and ductility, as well as resistance to general, pitting and stress corrosion cracking **[L. 1–3, 6–9]**. These steels, due to their characteristic properties, are used in many industry sectors worldwide. Thanks to their corrosion resistance, they are used in flue gas desulphurization. In addition, they are also used in structures and installations for seawater desalination, in the paper and pulp industries. They are used in the chemical industry, for heat exchanger components. One of the most important areas of application is in the marine industry, where it is used in the construction of ships for transporting chemicals **[L. 10, 11]**. The inherent process that accompanies all these constructions and installations is the welding process. The welding technology of duplex steel in large-scale structures poses many problems, which is why few centers in the world have taken the risk of producing chemical transport vessels made of this steel **[L. 12, 13]**. Phase transformations as well as precipitation processes of intermetallic phases, carbides, nitrides occurring in duplex steel during heating and cooling make it difficult to obtain adequate properties of welded joints **[L. 6, 8, 14, 15]**. A serious limitation in welding is the occurrence of embrittlement at 475°C **[L. 16]**, moreover, during the placement of successive stitches in the heat affected zone and the weld, transformations take place $\delta \rightarrow \gamma$ and $\gamma \rightarrow \delta$. As a result, more ferrite is observed, which has an adverse effect on the ductile properties of the joint and on corrosion resistance. Achieving high mechanical properties and corrosion resistance of joints is possible by observing the technological parameters of welding **[L. 17, 18]**.

The aim of this study is to analyze the microstructure and mechanical properties of welded joints for austenitic-ferritic duplex steel.

STUDY MATERIAL AND METHODOLOGY

In this study, welded joints of austenitic-ferritic duplex stainless steel X2CrMnNiN21-5-1 are investigated. The chemical composition of the steel according to the standards is presented in **Table 1**. The joint of sample 1 was made by welding with a rutile lagging electrode using the SMAW method. A 2.5 mm diameter ELGA CROMAROD DUPLEX electrode was designed for welding steels with low carbon content and high alloying elements (austenitic, ferritic-austenitic steels). The weld had t hree sequentially overlapped stitches. Welding was carried out at 85A and a voltage in the range 20–30 V. The joint of sample 2 was made using the GTA method in four passes. During the welding process, supplementary material in the form of uncoated OK TIGROD 2209 electrodes designed for welding duplex steels was used. The process was carried out under the following conditions of 11 V and 85 A.

Tests on welded joints included metallographic (macroscopic and microscopic), mechanical (static bending test, microhardness measurements), diffraction, and wear resistance tests.

Observations of welded joint microstructures were made with a Leica DMLM 4000M light microscope on etched metallographic specimens. The specimens were properly prepared and electrolytically etched in a reagent consisting of: 40 g NaOH and 100 mm^3 H_2O, voltage 2 V, etching time 10–20 seconds, at room temperature. This made it

Table 1. Chemical composition of base material X2CrMnNiN21-5-1 in accordance with PN-EN 10088-1: 2014-12 [L. 19]
Tabela 1. Skład chemiczny dla materiału X2CrMnNiN21-5-1 zgodnie z normą PN-EN 10088-1: 2014-12 **[L. 19]**

Grade of steel	C	Cr	Mn	Ni	Si	P	Mo	Cu	N
X2CrMnNiN21-5-1	<0.04	21-22	4-6	1.35-1.7	<1	<0.04	0.1-0.8	0.1-0.8	0.22

possible to reveal the fusion lines and the limits of the heat-affected zone (HAZ). Microstructures were observed in the weld, in the HAZ and in the region of the base material. The metallographic study was preceded by macroscopic observations using a stereo microscope. In addition, the surface of the samples was observed after wear resistance testing using a Phenom XL scanning electron microscope.

The static bending test was carried out in accordance with PN-EN ISO 5173:2023-06 **[L. 20]**. The samples were 100 x 6 x 15 mm cuboids (**Figure 1**), which were cut out of the welded joint, the weld face and root were removed and then lateral bending was applied. The bending mandrel test was performed by locating the samples on two supports formed by two parallel rollers. The sample was positioned so that the weld zone was centered between the support rollers. The material was bent so that at the center of the span the force increased gradually in a continuous manner from the bending pin in the weld axis to the surface of the sample.

Microhardness measurements were carried out in accordance with PN-EN ISO 9015:2011 **[L. 21]** using an Innovatest hardness tester by the Vickers method at a load of 1kG (HV1). Hardness measurements of welded joints were carried out on samples taken transverse to the weld axis. For

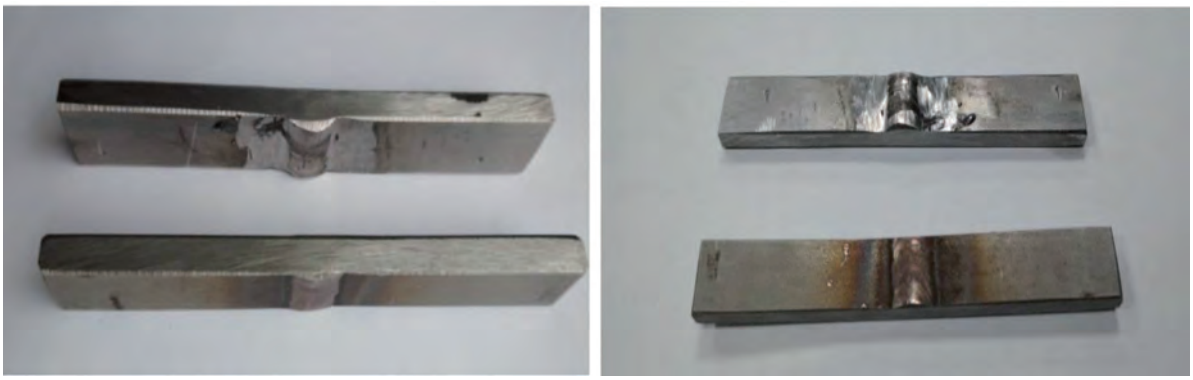

Fig. 1. Samples used in the bending test
Rys. 1. Próbki zastosowane w próbie zginania

sample 1, imprints were made in two measurement lines passing through the base material, HAZ and weld, at 1 mm intervals. Both lines were 2 mm from the surface of the sheet, while for sample 2, measurements were made in only one line from the face.

An X-ray diffractometer D8 Advance from Brucker equipped with a cobalt anode lamp λ_{Co} = 0.17902 nm was used. The following measurement conditions were established:
- angular range 2 θ = 40°–130° ,
- step Δ2 θ = 0.04°,
- time τ = 5 s/step

The wear tests were carried out with a T-05 block-on-ring tester (ITEE, Poland). The wear test conditions were as follows:
- dimensions of the test sample: 20 x 4 x 4 mm,
- rotating ring: heat-treated steel 100Cr6, 53 HRC, Ø49.5 x 8 mm,
- rotational speed: 200 rpm,
- load: 100 N,
- sliding distance: 500 m.

The coefficient of friction was defined as the ratio of the average frictional force (expressed in Newtons) to the load, expressed in Newtons.

RESULTS

The results of the macroscopic metallographic examination are shown in **Figure 2**, and the microscopic examination in **Figures 3–6**. The sample for metallographic examination was cut perpendicular to the welding direction. The individual stitches are visible. The double-stranded weld is characterized by a relatively large face width of about 14mm (**Figure 2a**) and symmetry with respect to the weld axis. Analyzing the macroscopic cross-sections of the joints, it can be seen that, in the case of the joint of sample number 1, a symmetrical weld and excessive reinforcement

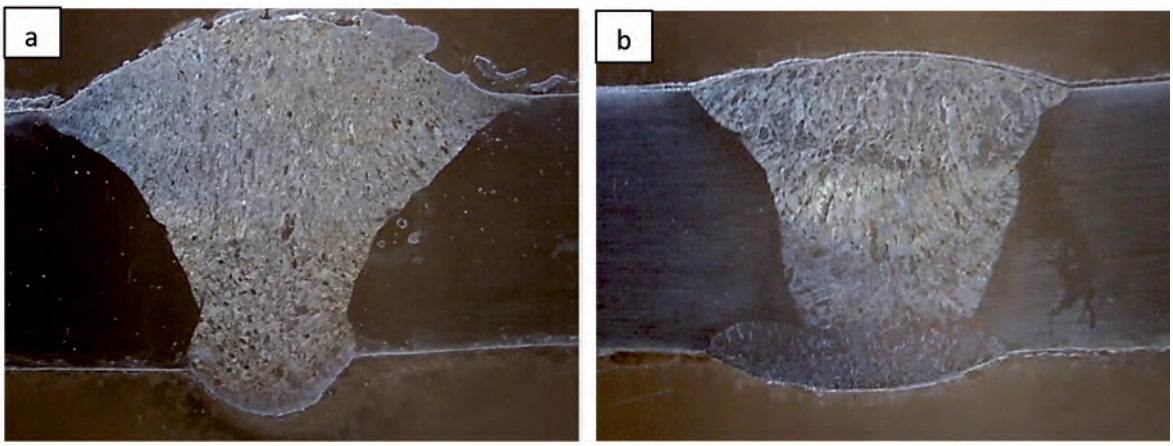

Fig. 2. Macrostructure of the welded joint of X2CrMnNiN21-5-1: steel sample 1 (a), sample 2 (b)
Rys. 2. Makrostruktura złącza spawanego stali X2CrMnNiN21-5-1: próbka numer 1 (a), próbka numer 2 (b)

(502) and root penetration (504) are observed. These are discrepancies meeting quality level C according to PN-EN ISO 5817:2023-08 **[L. 22]**. Spatters (602) on the face side are also visible. In the case of sample number 2 (Figure 2b), the face on both sides of the joint meets quality level B according to PN-EN ISO 5817:2023-08 **[L. 22]**.

Figure 3 shows the banded structure of the base material of ferritic-austenitic steel, the bands of both phases being oriented parallel to the rolling plane. The bright elongated austenite grains are located against the dark matrix, which is ferrite. The volume proportion of ferrite determined by X-ray was 53% and of austenite 47%.

Approaching the HAZ, the disappearance of elongated austenite and ferrite bands is observed (**Figure 4**). **Figure 5a–c** presents the microstructure showing the individual stitching occurring in the weld of sample 1. The microstructure of the weld is clearly different from the microstructure of the base material. The banded nature of the structure disappears, but the two phases – light austenite and dark ferrite – are still present. The amount of both phases and the morphology changes. In the first and second stitch (**Fig. 5 a–b**), austenite separations in the form of dendrites against a background of dark ferrite are visible, while in the third stitch, needle-like austenite separations are observed, which are distributed in the ferrite. The amount of ferrite in the weld compared to the base material decreased by 20% and is approximately 33%. A similar relationship was described by Liu et al. **[L. 23]. Figure 6** shows the microstructure of the weld metal of sample 2. Three austenite morphologies were observed: plate-like grain boundaries (**Fig. 6b**), intra-grain, which takes the form of parallelograms

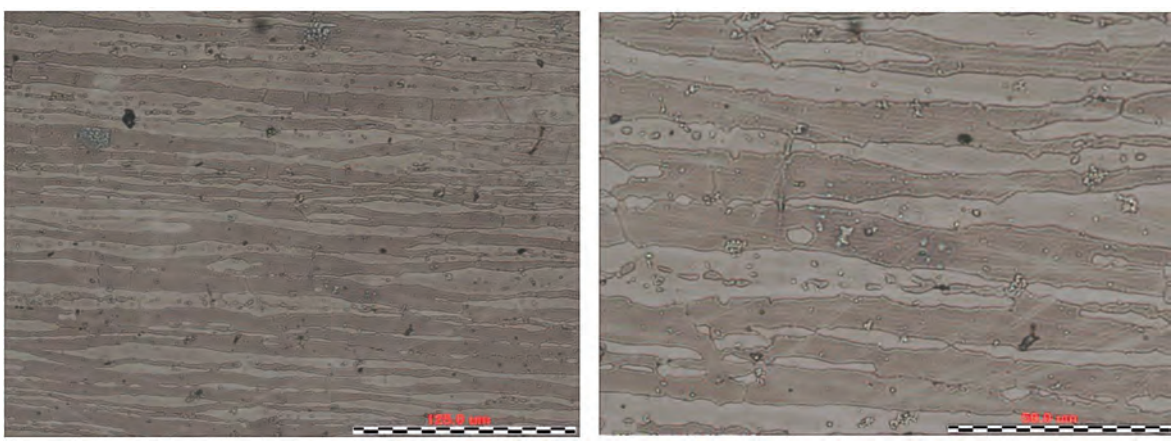

Fig. 3. Microstructure of the base material of X2CrMnNiN21-5 steel
Rys. 3. Mikrostruktura materiału rodzimego stali X2CrMnNiN21-5

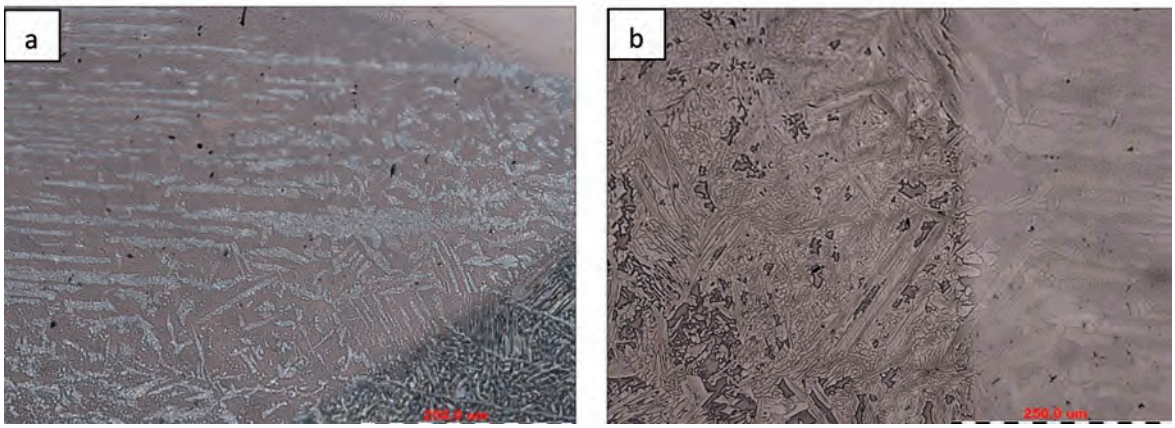

Fig. 4. Microstructure of the area at the BM/HAZ: boundary sample 1 (a), sample 2 (b)
Rys. 4. Mikrostruktura obszaru na granicy MR/SWC: próbka numer 1 (a), próbka numer 2 (b)

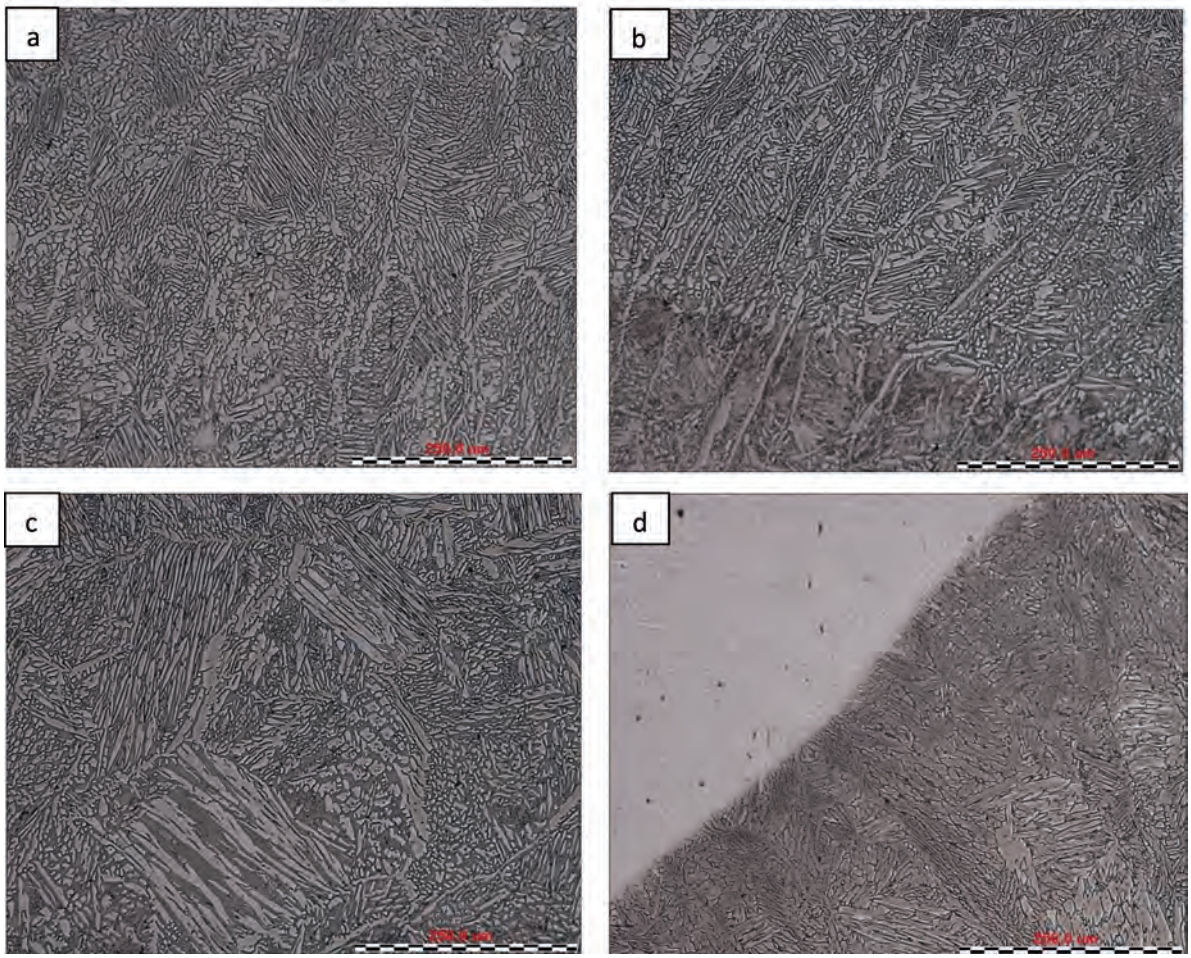

Fig. 5. Microstructure: stitch one (a), stitch two (b), stitch three (c), fusion line and HAZ (d) sample 1
Rys. 5. Mikrostruktura: ściegu pierwszego (a), drugiego (b), trzeciego (c), linii wtopienia i SWC (d) próbka numer 1

(**Fig. 6b**) and needle-like austenite separations in a Widmanstatten system against a background of ferrite (**Fig. 6d**). The amount of ferrite determined by X-ray is 54% and is comparable to that in the native material.

Austenite forming in the weld has a wide range of morphologies, and the microstructure of previously aligned stitches may be altered by reheating during multi-run welding. The phase transitions occurring during reheating and cooling

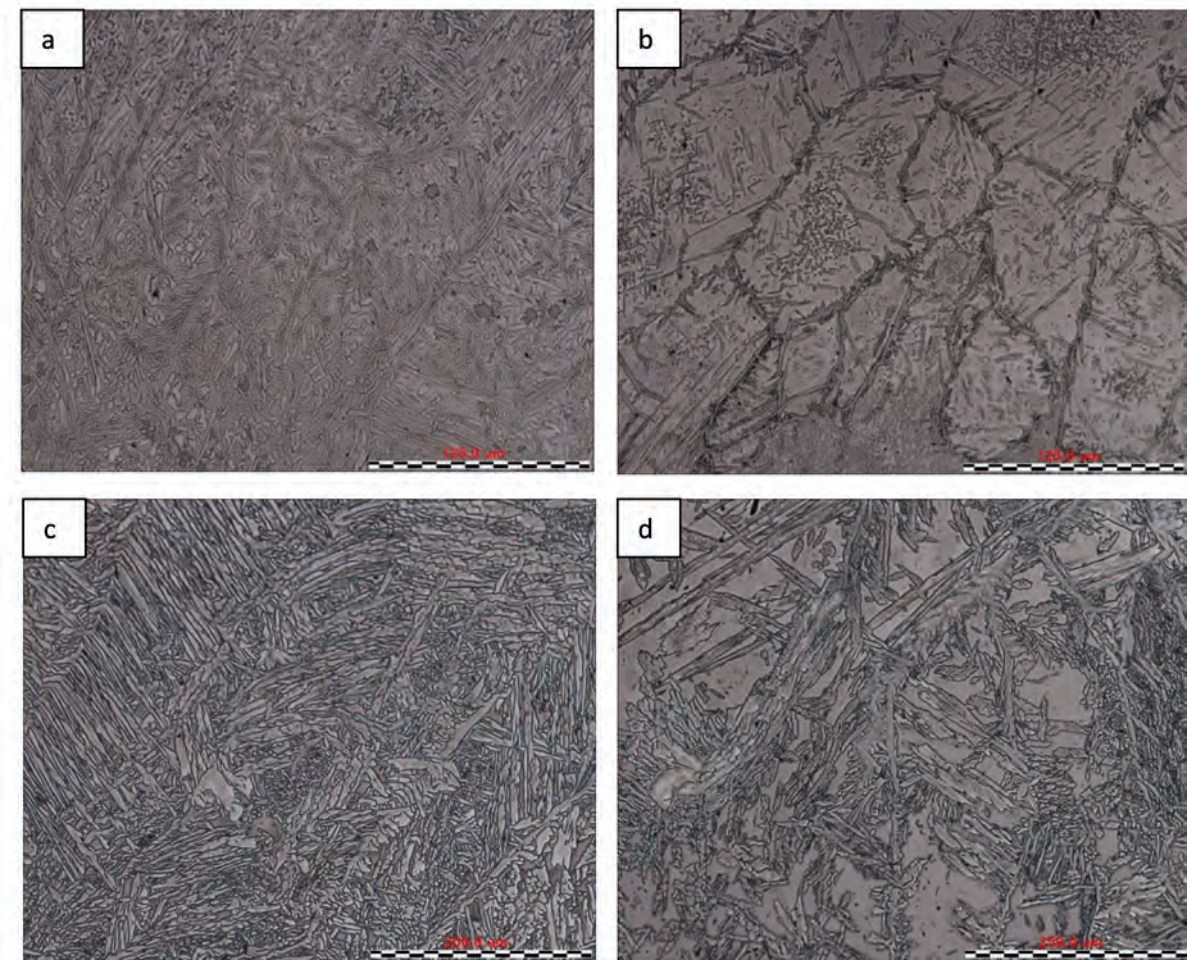

Fig. 6. Microstructure of stitch: one (a), stitch two (b), stitch three (c), stitch four (d) sample 2
Rys. 6. Mikrostruktura ściegu: pierwszego (a), drugiego (b), trzeciego (c), czwartego (d) próbka numer 2

have a significant effect on the structure, phase composition, phase morphology and, thus, the mechanical properties of the welded joint. During welding, phase transformations $\delta \rightarrow \gamma$ and $\gamma \rightarrow \delta$ occur in the heat affected zone and the weld as a result of the high temperature during the deposition of successive stitches.

The static bending test was carried out using the three-point transverse bending method with a bending pin. When the samples were bent,

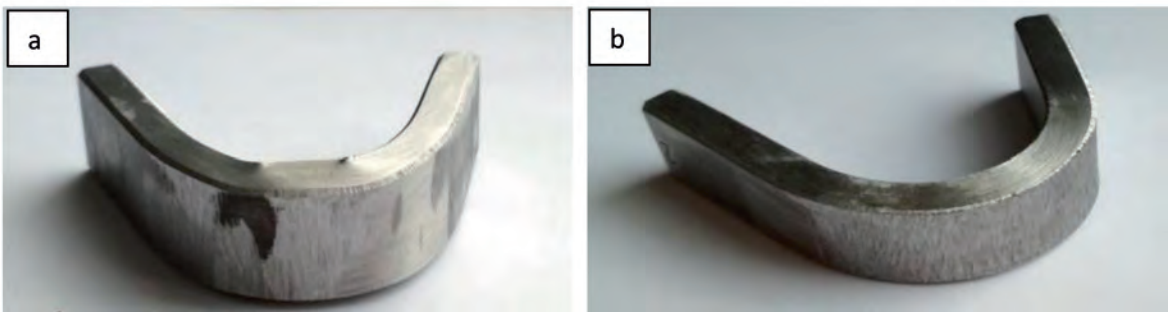

Fig. 7. Samples after the bending test from the tensile side: sample 1(a), sample 2 (b)
Rys. 7. Próbki po próbie zginania od strony rozciągania: próbka numer 1(a), próbka numer 2 (b)

a bending angle of 160° was achieved in both cases, indicating good plastic properties of the welded joint. No defects disqualifying the joint were observed on the surfaces subjected to tensile stress.

Figure 8 shows the results of microhardness measurements, which were carried out using the Vickers method in two rows – from the face side and from the boundary side for sample 1 and from the face side for sample 2. The results of microhardness measurements in the area of the base material are characterized by similar HV1 values. A slight increase is observed in the weld area, which may be due to the morphology (fragmentation) of the crystallizing phases in the weld. The microhardness of the weld face of sample 1 varies from 258 to 272 HV1, while that of sample 2 varies from 261 to 277 HV1.The microhardness values measured from the boundary side for sample 1 do not differ much from those from the face side – they are in the range 254–271 HV1. The lowest measured hardness for sample 1 is 232 HV1 and lies just outside the heat affected zone on the boundary side, and the highest is 272 HV1 and lies within the weld on the face side. For sample 2, the lowest measured hardness is 229 HV1m just outside the HAZ, and the highest is 278 HV1 and it is located in the weld zone. Measurements in this sample are made from the face side.

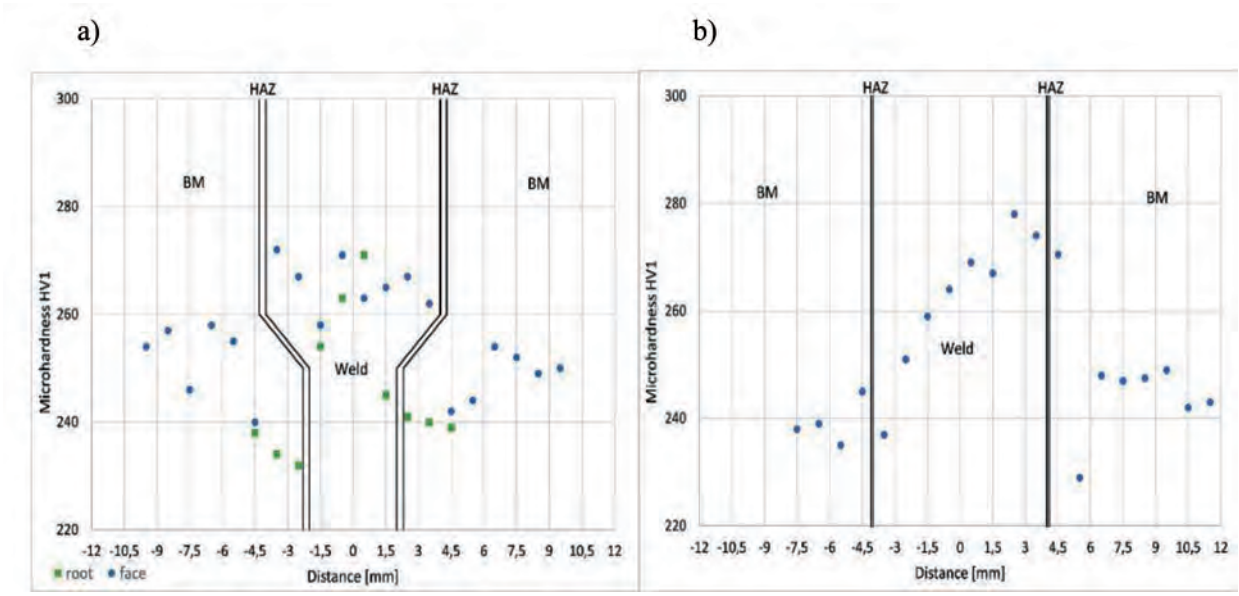

Fig. 8. Microhardness changes in the weld, HAZ and BM measured from the face and boundary of sample 1 (a), from the face of sample 2 (b)

Rys. 8. Zmiany mikrotwardości w spoinie, strefie wpływu ciepła (SWC) i materiale rodzimym (MR) zmierzone od strony lica i grani: próbka numer 1 (a), od strony lica próbka numer 2 (b)

The X-ray phase and diffraction line profile analyses made it possible to study the phase composition and any changes in the weld in relation to the base material. **Figure 9a** shows the diffraction record of the base material, while **Figure 9b** and **9c** show the record made within the weld for sample 1 and sample 2, respectively. All diffractograms show peaks originating from both austenite and ferrite. In the base material, the highest peak is (110)δ. Next to it, there is also a strong line coming from (111)γ. In addition, there are other lines from ferrite and austenite that are much smaller. In the weld of sample 1, the highest lines are (111)γ and (110)δ. Next to these, there is a relatively high (200)γ peak. In the weld of sample 2, the highest line is from ferrite (110)δ. There is also a strong peak from (111)γ. The reflection intensity ratios for austenite $I_{\gamma 111}/I_{\gamma 200}$ and for ferrite $I_{\delta 110}/I_{\delta 200}$ were calculated and compared with the theoretical values for the PDF standard from the ICDD database. Analysis of these simple indices makes it possible to determine the presence and strength of crystallographic texture. The results are shown in **Table 2.** The occurrence of differences between the theoretical value and the experimentally determined intensity ratios prove the thesis about material texturing.

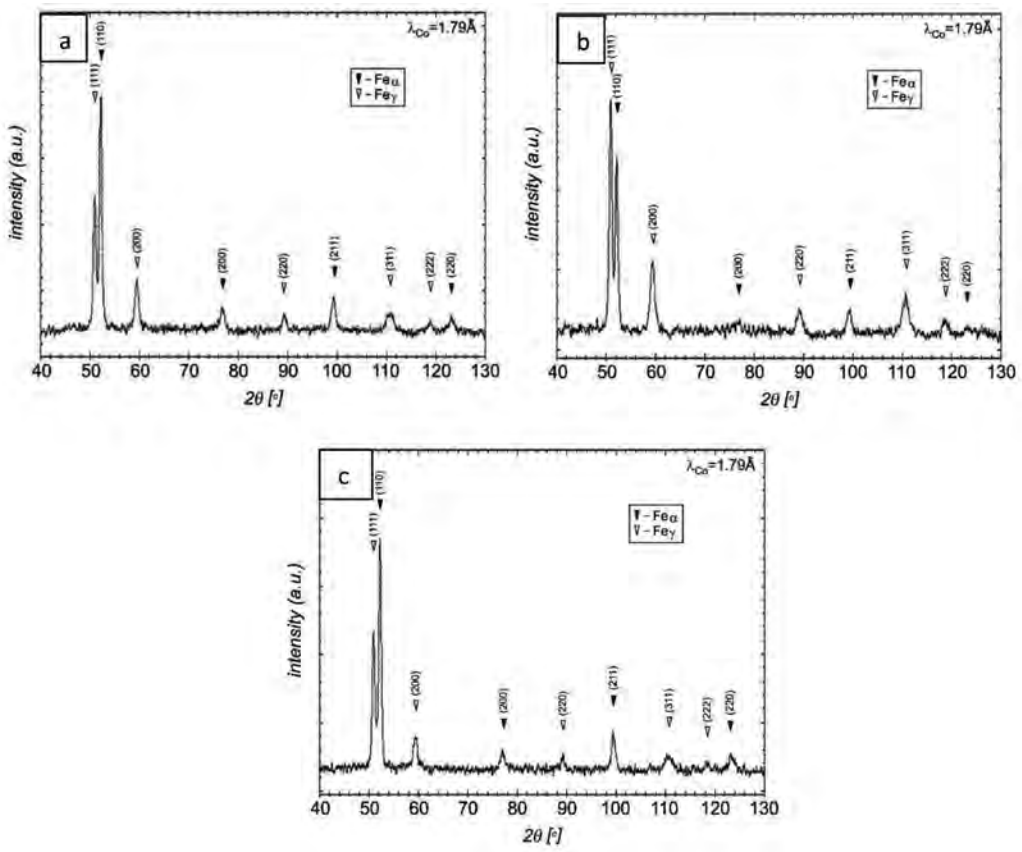

Fig. 9. Diffractogram of the base material of X2CrMnNiN21-5 steel (a), weld sample 1 (b), weld sample 2 (c)
Rys. 9. Dyfraktogram materiału rodzimego stali X2CrMnNiN21-5 (a), spoiny próbka numer 1 (b), spoiny próbka numer 2 (c)

Table 2. Intensity ratios for the pattern (non-textured) and study samples
Tabela 2. Stosunki intensywności dla materiału próbki wzorcowej (o bezładnej orientacji) i badanych próbek

Sample	$I_{\gamma 111}/I_{\gamma 200}$	$I_{\delta 110}/I_{\delta 200}$
Pattern	2	5
Base metal	2.9	7.5
Weld area-sample 1	2	16.8
Weld area-sample 2	2	6.4

Observations of the surface after the tribological test indicate clear differences in the wear mechanism between the base material and the welded area (**Figures 10–12**). In the case of the base material, wear occurs mainly by an abrasive mechanism. In the case of abrasive wear, the micro-cutting mechanism predominates, but there is also scratching including grooving effects. In the next stage of the grooving phenomenon, the plastically deformed material is then rolled and crumbled (**Fig. 10**). Locally, characteristic adhesive wear effects can also be observed. In the case of the weld area, in addition to wear mechanisms similar to those in the base material, crumbles plays a major role. This is facilitated by an increase in hardness and finer grain size with a conifer-like morphology. This is favored by microcracking along the fine precipitates of the ferrite δ, especially with its Widmanstatten-like morphology. This is also favored by the continuous lattice of these precipitates, as seen most clearly in **Figure 6b**. Changes in coefficients of friction with the length of the test indicate a change in wear mechanisms, until the above-mentioned mechanism stabilizes (**Figure 13a**). The base material stabilizes during the tribological test with a slight increase in this coefficient. This may indicate the activation of adhesive wear at a later stage of the tribological test, as well as the incorporation of a third material body into the friction system in the form of crumbling fragments of plastically deformed material due to grooving. The changes in the coefficient of friction have a different character for the weld areas (**Fig. 13a**). Stabilization of this coefficient occurs as its value decreases. This is probably related to the activation of the material crumbling mechanism.

The crumbling of the material in this case, by exceeding its cohesion forces, reduces the friction forces. This mechanism results in a slightly lower coefficient of friction for the weld area compared to the base material at the end of the test. On the other hand, looking at the average value of the coefficient of friction (**Fig. 13b**), the highest occurred for weld material 1. This may be related to the large difference between the hardness of the weld and the reduced hardness in terms of the effect of heat on the plastically deformed base material (recrystallisation). This combination of soft areas easily subjected to abrasive wear and hard areas easily subjected to crumbling results in the highest mass wear (**Fig. 13c**). The grooving mechanism causes less mass wear, resulting in the least wear on the base material, as shown in **Fig. 13c**.

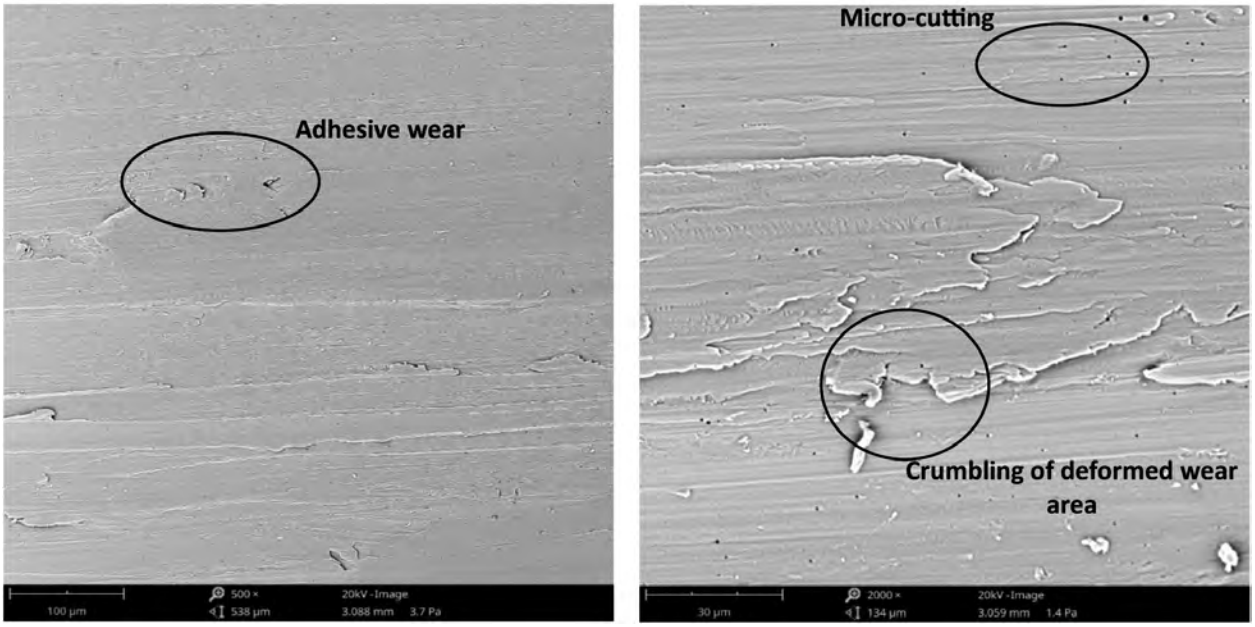

Fig. 10. Surface of base metal after examining wear resistance
Rys. 10. Powierzchnia materiału rodzimego po badaniu trybologicznym

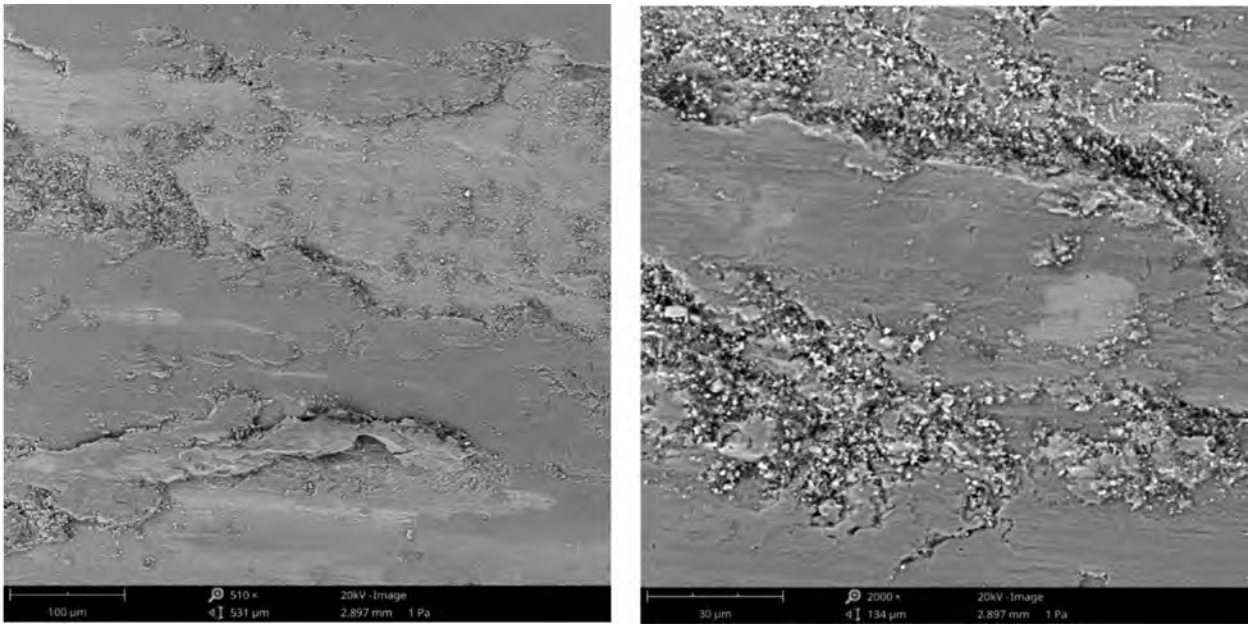

Fig. 11. Surface of sample 1 after examining wear resistance
Rys. 11. Powierzchnia próbki 1 po badaniu trybologicznym

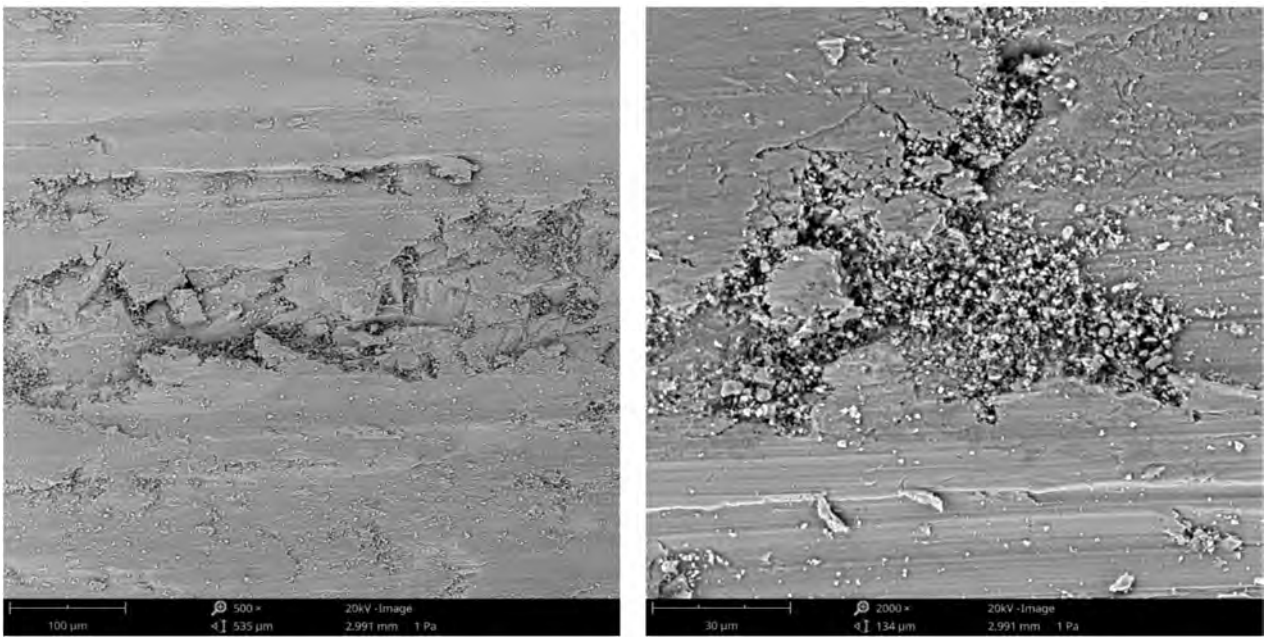

Fig. 12. Surface of sample 2 after examining wear resistance
Rys. 12. Powierzchnia próbki 2 po badaniu trybologicznym

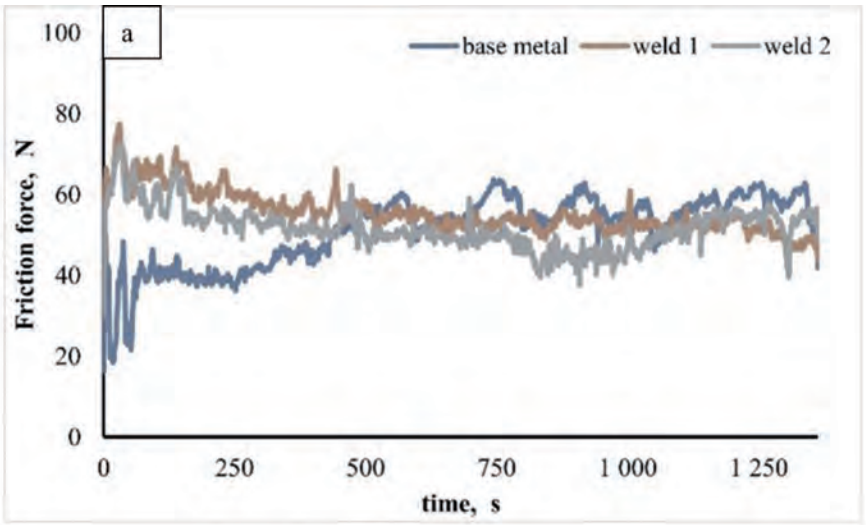

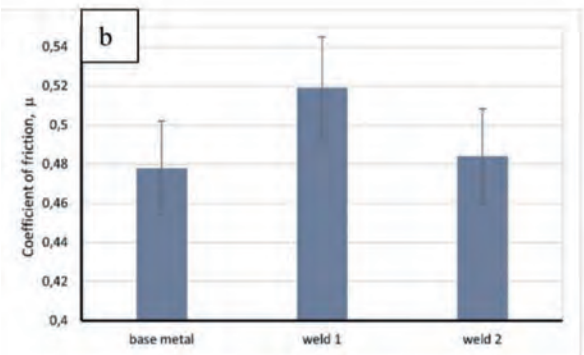

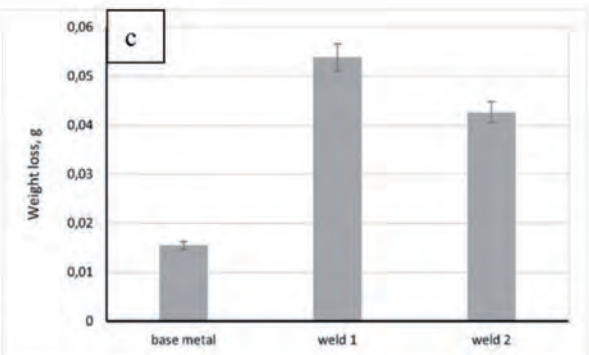

Fig. 13. Effect of material type o n friction force (a), coefficient of friction (b), and weight loss (c)
Rys. 13. Wpływ rodzaju materiału na siłę tarcia (a), współczynnik tarcia (b) i ubytek masy (c)

CONCLUSIONS

- There are two phases, austenite (γ) and ferrite (δ), in the microstructure of the joint of both samples, with different morphologies depending on the welding conditions that influence the phase transformations.
- The weld is relatively ductile as confirmed by the bending test.
- The microhardness of the welds of both samples is similar, averaging 252 HV1, regardless of the welding production technique.
- Diffraction phase analysis shows that the material is textured, especially ferrite, as there are differences in intensity ratios between the reference sample and the tested materials.
- Wear resistance tests show that there is more material wear in the weld area than in the base material.

The work was financed by the Ministry of Science and Higher Education within the framework of the research subvention of the AGH University of Science and Technology in Cracow No. 16.16.110.663 , No. 16.16.130.942

REFERENCES

1. Davis, J.R.: Alloy Digest Sourcebook Stainless Steels. ASM International: Materials Park, OH, USA, 2000.
2. Lamb S. ed.: Casti handbook of stainless steels&nickel alloys. Casti Pub., Canada, 2002.
3. Alvarez-Armas I.: Degallaix-Moreuil S. Duplex Stainless Steels. Wiley: Hoboken, NJ, USA, 2009.
4. Sieurin H., Sandström R., Westin E.M.: Fracture toughness of the lean duplex stainless steel LDX 2101, Metall. Mater. Trans. A 37, 2006, 2975-2981.
5. Francis R., Byrne G.: Duplex stainless steel-alloys for the 21st Century, Metals, 11, 836, pp. 1–23.
6. Ghosh S.K., Mondal S.: High temperature ageing behaviour of a duplex stainless steel. Materials Characterization 59, 2008, pp. 1776–1783.
7. Bernhardsson S.: The corrosion resistance of duplex stainless steels, Duplex Stainless Steels'91, vol. 1, 1991, pp. 185–210.
8. Chen T.H., Weng K.L., Yang J.R.: The effect of high-temperature exposure on the microstructural stability and toughness property in a 2205 duplex stainless steel, Materials Science Engineering A 338 (1–2), 2002, pp. 259–270.
9. Moura VS., Lima LD., Pardal JM., et al: Influence of microstructure on the corrosion resistance of the duplex stainless steel UNS S31803. Materials Characterization, 2008, 59, pp. 1127–1132.
10. Weibull Ivar: Duplex stainless steels and their application, particularly in centrifugal separators: Part A. History and development. Mater Des 1987, 8, pp. 35–40.
11. Weibull Ivar: Duplex stainless steels and their application, particularly in centrifugal separators: Part B. Corrosion resistance. Mater Des 1987, 8, pp. 82–88.
12. Nowacki J.: Duplex steel and its weldability, WNT, Warsaw 2009.
13. Nowacki J.: Duplex steel in welded structures, WNT, Warsaw 2013.
14. Badjia R., Bouabdallahb M., Bacroixa B., Kahlouna C., Belkessac B., Maza H.: Phase transformation and mechanical behaviour in annealed 2205 duplex stainless steel welds, Materials.
15. Karlsson L., Wessman S., Fuertes N.: Effect of sigma phase morphology on the degradation of Characterization 59, 2008, pp. 447–453.
16. Hosseini V., properties in a super duplex stainless steel, Materials, 2018, 11, 933, pp. 1–20.
17. Hosseini V.A., Thuvander M., Lindgren K., Oliver J., Folkeson N., Gonzalez D., Karlsson L.: Fe and Cr phase separation in super and hyper duplex stainless steel plates and welds after very short aging Times, Materials & Design, 2021, 210, pp. 1–11.
18. Tasak E.: Metallurgy of welding, JAK, Krakow 2008.

19. Tasak E.: Weldability of steel, Fotobit, Krakow 2002.
20. EN 10088-1: 2014-12 Corrosion resistant steels – Part 1: List of corrosion resistant steels.
21. PN-EN ISO 5173: 2023-06 Destructive testing of welds in metallic materials – Bend test.
22. PN-EN ISO 9015:2011 Destructive testing of welded metal joints – Hardness testing – Part 1: Hardness testing of arc-welded joints.
23. EN ISO 5817:2023-08 Welding – Welded joints of steel, nickel, titanium and their alloys (except beam welded) – Quality levels for weld imperfections.
24. Liu J., Niu H., Zhang Y., Sun X.: Research on welding process of duplex stainless steel S31803, Journal of Physics: Conference Series, 2469, 2023, pp. 1–6.